Experimental Evaluation of Characteristic of Switched Reluctance Motor Made by Blanking Amorphous Alloy Foil

Takahiro Kumagai [1], Hirotaka Sakurai [1*], Jun-ichi Itoh [1], Keisuke Kusaka [1], Takashi Yamaguchi [2], Masayuki Nakagawa [3], and Daisuke Sato [4]

[1] Department of Electrical, Electronics and Information Engineering, Nagaoka University of Technology, Japan
[2] Yamaguchi Manufacturing Co., Ltd., Japan, [3] Industrial Research Institute of Niigata Prefecture, Japan,
[4] Nagaoka Motor Development Co., Ltd., Japan

***Abstract*—This paper provides the characteristics of switched reluctance motors (SRMs) made by blanking (a) 20H1300 of high grade low-iron-loss silicon steel (0.20mm thickness) and (b) 2605SA1 of amorphous alloy (0.025mm thickness). As first prototype, 70W-SRM (40mm thickness) is manufactured by blanking 1600 sheets of amorphous alloy and adhesively laminating them. In experiment, the motor efficiency of amorphous-alloy-SRM is improved by 6.4p.t. compared with that of silicon-steel-SRM. In addition, the iron loss of amorphous-alloy-SRM is reduced by 61.9% compared with that of silicon-steel-SRM.**

***Index Terms*—Switched reluctance motor (SRM), amorphous alloy foil, blanking, iron loss**

I. INTRODUCTION

Due to an increasing awareness of environmental issues, high-efficiency motor and high-power density motor for home appliances, industrial application, and electric vehicles have been actively studied and developed [1-5]. In order to achieve the higher power density, the electric motor is operated at higher speed. High speed operation has become easier with the practical use of wide bandgap semiconductor such as silicon carbide (SiC) and gallium nitride (GaN). However, high speed operation deteriorates the motor efficiency due to the iron loss which is increased depending on the electrical frequency.

Amorphous alloy has attracted much attentions thanks to its low iron loss properties. In the amorphous alloy, the eddy current loss is small because it is thin and high electrical resistivity. In addition, the hysteresis loss is also small because it has no crystal structure [6]. So far, there are many researches to apply the amorphous alloy into the core of classic motors such as permanent magnetic synchronous motor (PMSM) [7-11], induction motor (IM) [12], and switched reluctance motor (SRM) [13-15]. In particular, Ref.[15] has reported that the iron loss of motor core was reduced by about 80% compared with 35A300 of a general low-iron-loss silicon steel with the employment of amorphous alloy. In addition, the efficiency of this amorphous alloy motor achieved more than 95% at an output of about 2kW thanks to its low iron loss properties. However, due to the difficulty in machining amorphous alloy, wire electrical discharge machining (WEDM), laser cutting, or chemical etching is adopted as a cutting method of amorphous alloy foil. These cutting processes lead to increasing of manufacturing cost and become an obstacle of mass production of an amorphous alloy motor. As the researches for the mass production of the amorphous alloy motor, there are two different approaches; (i) improvement of motor structure in order to avoid the complicated cutting process or (ii) improvement of blanking technology.

In approach of (i), the simplification of motor structure have been studied for avoidance of complicated cutting process. Ref.[16-23] have focused on an axial-gap motor whose stator core is a cylinder with a uniform cross-section shape in the axial direction, where it is comparatively easy to manufacture with the amorphous alloy. In particular, Ref.[22] has already commercialized the amorphous alloy axial-gap motor which satisfies the IE4 efficiency class. In addition, IE5 efficiency class is achieved with improved amorphous alloy axial-gap motor in Ref.[23]. However, these approaches still limits the applicability of an amorphous alloy.

In approach of (ii), the cutting of amorphous alloy foil has been attempted with the development of mold processing machines and technologies [24-30]. Ref.[28] has been reported that amorphous alloy foil was successfully blanked into a motor stator shape. In Ref.[29], high-speed blanking of amorphous alloy foil has been conducted and evaluated. Ref.[30] has presented the blanking results of the amorphous alloy stacks laminated by 20 layers. However, as far as the author knows, there is no instance to manufacture the entire motor by blanking amorphous alloy foil. The establishment of blanking technologies of amorphous alloy is expected in order to expand the application of the amorphous alloy more widely

In this paper, as one attempt in approach of (ii), a switched reluctance motor (SRM) is manufactured by blanking the amorphous alloy and evaluated in the experiment. As first prototype, 70W-SRM (40mm thickness) is manufactured by blanking 1600 sheets of the amorphous alloy and adhesively laminating them. In addition, the same designed SRM is manufactured by blanking silicon steel for comparative verification. In this paper, the iron loss characteristic and motor efficiency

characteristic of the manufactured SRMs are experimentally evaluated.

II. Pre-experimental Evaluation of Ring Cores

As a preliminary step of the experimental evaluation with motor, the iron loss characteristics of the cores made by different material and processing method are evaluated with ring core. Generally, the evaluation of the iron loss with ring core is more basic and more accurate.

Table.1 shows the specifications of the ring cores, whereas Fig.1 shows the photograph of the manufactured ring cores. Four ring cores are manufactured in order to evaluate the iron loss characteristics of the cores made by the different material and the processing method. Two ring cores are made by the laser cutting after laminating (a) 20H1300 of the high grade low-iron-loss silicon steel (0.20mm thickness) and (b) 2605SA1 of the amorphous alloy (0.025mm thickness), which are referred as "SS-C" and "AA-C" in this paper. The others are made by laminating after blanking (a) 20H1300 and (b) 2605SA1, which are referred as "SS-B and "AA-B in this paper.

Fig.2 depicts the diagrams of the measurement setup for the ring core. The primary and secondary windings with the same number of turns are wound around the manufactured ring core. The iron loss W_i and the amplitude of magnetic flux density B are expressed as (1) and (2).

$$W_i = \frac{1}{T}\int_0^T i_1(t)v_2(t)dt \quad \text{.....(1)}$$

$$B = \frac{\sqrt{2}V_{2\_rms}}{2\pi f N_2 S_c} \quad \text{.....(2)}$$

where i_1(t) is the current in the primary winding, v_2(t) is the voltage of the secondary winding, f is the frequency of the applied sinusoidal voltage, N_2 is the number of turns in the secondary winding, S_c is the effective cross-sectional area of the ring core, V_{2_rms} is the root mean square value of v_2(t) at no-load test. The active power measured by the power meter in Fig.2, i.e. the time average value of instantaneous power expressed by (1), is equal to the magnetic energy consumed by the iron core.

Fig.3 shows the comparison results of the iron losses of the four ring cores. The sinusoidal voltage with the frequency of 1kHz is applied into the primary winding with the bipolar power supply. In regard to the difference in the characteristics depending on the material, the iron loss of the silicon steel are around 500W as shown in Fig.3(a), whereas the iron loss of the amorphous alloy are under 100W at 1.2T. Therefore, the iron loss of the amorphous alloy is over 80% lower that of the silicon steel. In regard to the difference in the characteristics depending on the processing process, the iron loss of the SS-B and the AA-B are increased by 10.9% and 10.7% respectively compared with that of the SS-C and the AA-C. This increases of the iron loss will be due to the properties degradation during the blanking processes. Note that the properties degradation is the almost same for both the silicon steel and the amorphous alloy, and neither is so

TABLE I
Specification of Ring-cores

Name of Ring core	SS-C	SS-B	AA-C	AA-B
Iron core	silicon steel (20HX1300)		amorphous alloy (2605SA1)	
Steel Thickness	0.20mm		0.025mm	
Processing Method	Wire cut After Laminated	Laminated After Blanking	Wire cut After Laminated	Laminated After Blanking
Lamination factor	97.5%	97.9%	94.5%	95.6%

Fig. 1. Photograph of ring-cores made with the processing method as shown in Table 1.

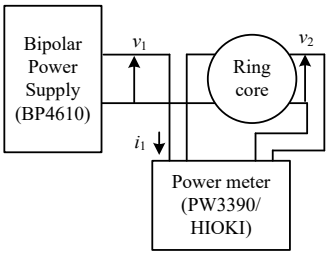

Fig. 2. Diagrams of measurement setup for ring-core

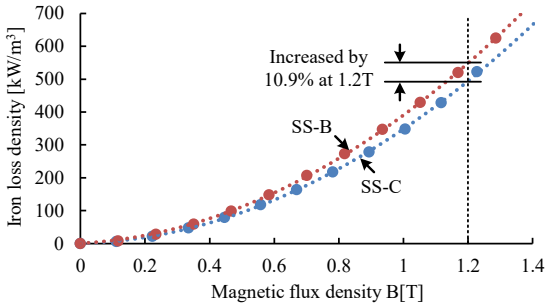

(b) Silicon steel

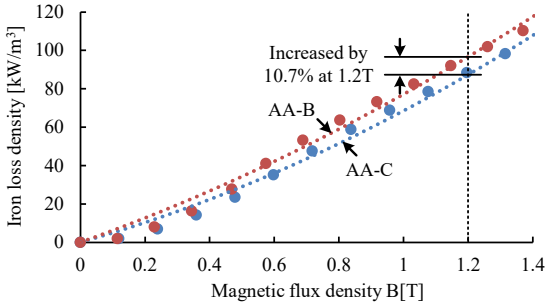

(b) Amorphous alloy

Fig. 3. Comparison results of iron losses at a frequency of 1kHz.

large. Therefore, the properties degradation due to blanking the amorphous alloy is not a serious problem in practical use.

III. Design and Manufacture of SRMs

Table.2 shows the specifications of the designed SRMs, whereas Fig.4 shows the photograph of the manufactured amorphous-allow-SRM. 70W SRMs (40mm thickness) are designed as first prototype. Two motor cores are made by blanking (a) 20H1300 and (b) 2605SA1, which are referred as "SS-SRM" and "AA-SRM" in this paper. The number of layers of the SS-SRM is 200, whereas that of the AA-SRM is 1600. These motors are manufactured by adhesively laminating the blanked steel sheets. In order to increase the effect of the iron loss reduction, a relatively high-speed motor is designed. In addition, the coil space is bigger than a general design [31] in order to increase the winding diameter. This results in low winding resistance and copper loss reduction. Furthermore, the airgap is designed to a very small value of 0.1mm in order to obtain large torque per current value.

IV. Experimental Evaluation of SRMs

A. Test System Configuration

Fig.5 (a) depicts the diagrams of the measurement setup for test motor, whereas Fig.5 (b) shows the photograph of the measurement bench. In particular, the motor efficiency characteristics and the iron loss characteristics of the SS-SRM and the AA-SRM are experimentally evaluated with the measurement bench. The input electric power is measured with the power meter (PW3390, accuracy±0.04%, bandwidth200kHz, HIOKI), whereas the torque is measured with the torque meter (UTMII-1Nm, accuracy±0.01%, bandwidth1kHz, UNIPULSE). The motor efficiency η_{motor} is expressed as (3).

$$\eta_{motor} = \frac{P_{out}}{P_{in}} \quad \text{.....(3)}$$

where P_{out} is the shaft output which is calculated as product of the measured torque and the shaft angular velocity, whereas P_{in} is the input electric power which is measured by the power meter. On the other hand, the iron loss W_i are calculated by subtracting P_{out}, the mechanical loss W_m, and the copper loss W_c from P_{in}. Therefore, W_i is expressed as (4).

$$W_i = P_{in} - P_{out} - W_c - W_m \quad \text{.....(4)}$$

$$where \quad W_c = \sum_{x=u}^{w} R_x I_{RMS\_x}{}^2 \quad \text{.....(5)}$$

where W_m is the product of the measured torque and the rotational angular velocity when the DC motor drives the system with no SRM excitation. R_x and I_{RMS_x} are the winding resistance and the root-mean-square (RMS) value of the winding current of x-phase respectively [15]. All measurements are conducted to keep the winding temperature within the range of 30 to 35 degrees. This is because W_m and W_c have temperature dependability.

TABLE II
Specification of Design SRM

Name of motor	SS-SRM	AA-SRM
Iron core	20H1300 (high grade silicon steel)	2605SA1 (amorphous alloy)
Number of layers	200 (cal.)	1600 (cal.)
Processing method	Laminated after Blanking	
Output power	70W	
Rated speed	7200r/min	
Rated torque	0.093Nm	
Input voltage	48V	
Number of phases	3	
Number of poles	6 (stator) / 4 (rotor)	
Motor size	40mm × 40mm	
Airgap	0.1mm	
Pole arc	21deg. (stator) / 31deg. (rotor)	
Number of turns	73turns	
Space factor of coil	34%	

Fig. 4. Photograph of 70W-SRM made of blanked amorphous alloy foil.

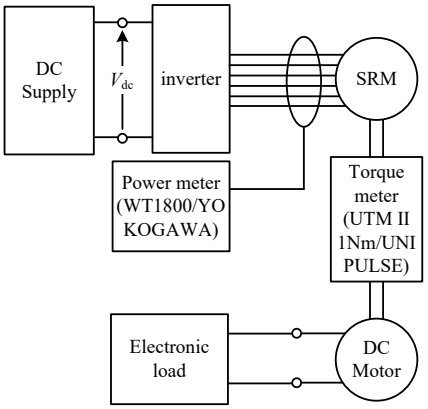

(a) Diagrams of measurement setup for test motor

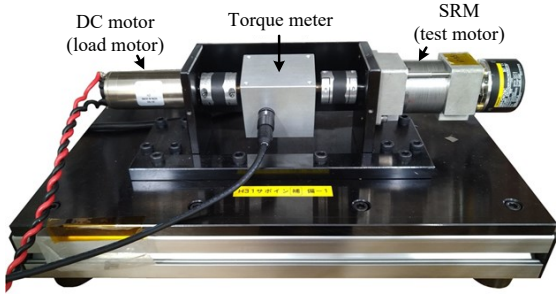

(b) Photograph of measurement bench

Fig. 5. Measurement system for test motor

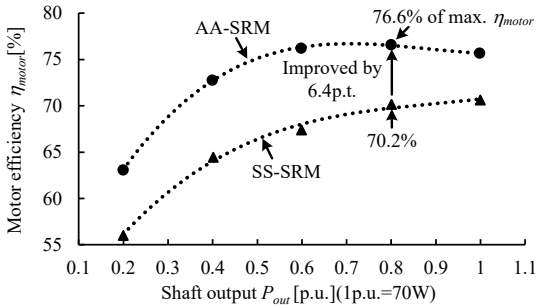

Fig. 6. Efficiency characteristics of SS-SRM and AA-SRM at rated speed.

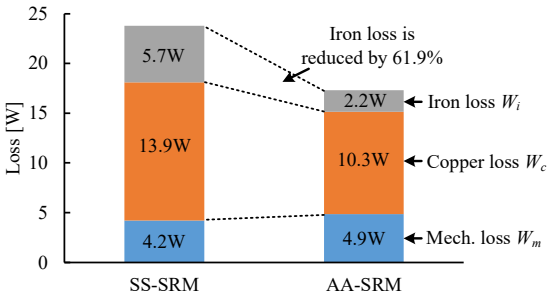

Fig. 7. Separation results of motor losses of SS-SRM and AA-SRM at 56W (0.8p.u.) of maximum efficiency point in Fig.2.

B. *Measured characteristics of SS-SRM and AA-SRM*

Fig.6 shows the motor efficiency characteristics of the SS-SRM and the AA-SRM. The shaft output is from 0.2p.u. to 1.0p.u. The rotation speed is rated speed. As shown in Fig.6, the motor efficiency of the AA-SRM is higher than that of the SS-SRM in all output range. In additon, the AA-SRM achieved the maximum motor efficiency of 76.6% at 56W (0.8 p.u.). At this operating point, the motor efficiency of the AA-SRM is improved by 6.4p.t. compared with that of the SS-SRM. Note that the motor efficiency of the AA-SRM is getting worse at rated output. This is because the amorphous alloy has lower maximum flux density as a sacrifice of low iron loss propeties, resulting in deterioration of the motor efficiency at relatively high torque range. However, the efficiency of the AA-SRM is still higher than that of the SS-SRM at rated output thanks to the iron loss reduction.

Fig.7 shows the separation results of the motor losses of the SS-SRM and the AA-SRM at 56W (0.8p.u.) of the maximum efficiency point as shown in Fig.6. As shown in Fig.7, the iron loss of the AA-SRM is reduced by 61.9% compared with that of the SS-SRM. Therefore, the iron loss reduction effect of the motor core is confirmed even in the blanked amorphous alloy. Note that this reduction rate of the iron loss will be lower than that reported in Ref.[15]. One of the reasons is that the silicon steel of our SS-SRM is 20H1300 of a high grade low-iron-loss silicon steel (0.20mm thickness), whereas that of the SS-SRM in Ref.[15] is 35A300 of a general low-iron-loss silicon steel (0.35mm thickness); the iron loss of the AA-SRM is compared with that of the SS-SRM whose iron loss is relatively low.

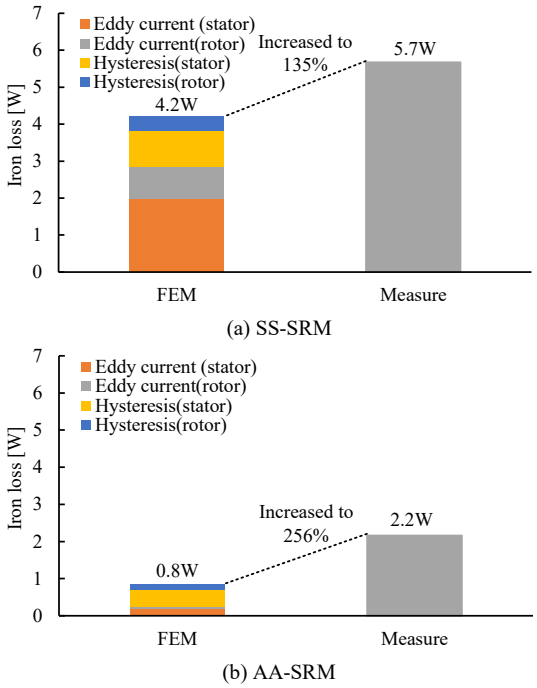

Fig. 8. Comparison results between FEA and measurement of iron losses at 56W (0.8p.u.) of maximum efficiency point in Fig.2.

C. *Comparison results between FEA and Measurement*

Fig.8 shows the comparison between the FEA results and the measurement results of the iron losses of (a) the SS-SRM and (b) the AA-SRM. The iron losses of the SS-SRM and the AA-SRM are calculated based on the measured iron loss curves of the ring cores of SS-B and AA-B respectively with 2D-FEM package (JMAG). As shown in Fig.8, the measured iron losses of the SS-SRM and the AA-SRM are increased to 135% and 256% respectively compared with those of the FEA results. It is confirmed that there is a great different characteristic between the FEA analysis and the measurement. One possibility of the cause of this difference is the low accuracy of iron loss analysis of FEA. It is mentioned that the simple iron loss calculation algorithm based on the iron loss curves is less accurate in case of the complicated magnetic flux waveforms of the SRM.

V. Conclusions

This paper provided the characteristics of the SRMs made by blanking (a) 20H1300 of the high grade low-iron-loss silicon steel (0.20mm thickness) and (b) 2605SA1 of the amorphous alloy (0.025mm thickness). As first prototype, 70W-SRM (40mm thickness) was manufactured by blanking 1600 sheets of the amorphous alloy and adhesively laminating them. In experiment, the motor efficiency of the amorphous-alloy-SRM was improved by 6.4p.t. compared with that of the silicon-steel-SRM. In addition, the iron loss of the amorphous-alloy-SRM was reduced by 61.9% compared with that of the silicon-steel-SRM. In the future, the characteristic of the motor made by blanking the amorphous alloy foil is evaluated more detailed in experiment and improved FEA.

REFERENCES

[1] Y. Enomoto, K. Deguchi, T. Imagawa, "Development of an Ultimate-high-efficiency Motor by utilizing High-Bs Nanocrystalline Alloy," IEEJ Journal of Industry Applications, vol. 9, no .1, pp. 102-108 (2020)

[2] T. Ogawa, T. Takahashi, M. Takemoto, S. Ogasawara, H. Arita, and A. Daikoku, "Increasing the Operating Speed of a Consequent Pole Axial Gap Motor for Higher Output Power Density," IEEJ Journal of Industry Applications, vol. 8, no. 3, pp. 497-504 (2019)

[3] U. U. Ekong, M. Inamori, and M. Morimoto, "Field-Weakening Control for Torque and Efficiency Optimization of a Four-Switch Three-Phase Inverter-Fed Induction Motor Drive," IEEJ Journal of Industry Applications, vol. 8, no. 3, pp. 548-555 (2019)

[4] K. Abe, H. Haga, K. Ohishi, Y. Yokokura, and H. Kada, "Source Current Harmonics and Motor Copper Loss Reduction Control of Electrolytic Capacitor-less Inverter for IPMSM Drive," IEEJ Journal of Industry Applications, vol. 8, no. 3, pp. 404-412 (2019)

[5] N. Miyauchi, "Reduction of the Power Consumption of a Stepping Motor for Driving the Hands of Wristwatches," IEEJ Journal of Industry Applications, vol. 8, no. 1, pp. 140-141 (2019)

[6] R. Tang, W. Tong, and X. Han, "Overview on amorphous alloy electrical machines and their key technologies," Chinese Journal of Electrical Engineering, vol. 2, no. 1, pp. 1–12 (2016)

[7] R. Kolano, A. Kolano-Burian, K. Krykowski, J. Hetmańczyk, M. Hreczka, M. Polak, and Jan Szynowski "Amorphous soft magnetic core for the stator of the high-speed PMBLDC motor with half-open slots," IEEE Transactions on Magnetics, vol. 52, no. 6, no. 2003005 (2016)

[8] S. Okamoto, N. Denis, Y. Kato, M. Ieki, and K. Fujisaki, "Core loss reduction of an interior permanent-magnet synchronous motor using amorphous stator core," IEEE Transactions on Industry Applications, vol. 52, no. 3, pp. 2261–2268 (2016)

[9] D.-K. Hong, D. Joo, B.-C. Woo, Y.-H. Jeong, and D.-H. Koo, "Investigations on a super high speed motor-generator for microturbine applications using amorphous core," IEEE Transactions on Magnetics, vol. 49, no. 7, pp. 4072–4075 (2013)

[10] T. Fan, Q. Li, and X. Wen, "Development of a high power density motor made of amorphous alloy cores," IEEE Transactions on Industrial Electronics, vol. 61, no. 9, pp. 4510–4518 (2014)

[11] W. Tong, S. Dai, S. Wu, and R. Tang, "Performance Comparison Between an Amorphous Metal PMSM and a Silicon Steel PMSM," IEEE Transactions on Magnetics, vol. 55, no. 6, no. 8102705 (2014)

[12] M. Dems and K. Komeza, "Performance characteristics of a high-speed energy-saving induction motor with an amorphous stator core," IEEE Transactions on Industrial Electronics, vol. 61, no. 6, pp. 3046–3055 (2014)

[13] F. Chai, Z. Li, L. Chen, and Yulong Pei, "Effect of cutting and slot opening on amorphous alloy core for high-speed switched reluctance motor," IEEE Transactions on Magnetics, pp. 1–5 (2020)

[14] H. Hayashi, K. Nakamura, A. Chiba, T. Fukao, K. Tungpimolrut, and D. G. Dorrell, "Efficiency improvements of switched reluctance motors with high-quality iron steel and enhanced conductor slot fill," IEEE Transactions on Energy Conversion, vol. 24, no. 4, pp. 819–825 (2009)

[15] A. Chiba, H. Hayashi, K. Nakamura, S. Ito, K. Tungpimolrut, T. Fukao, M. A. Rahman, and M. Yoshida "Test results of an SRM made from a layered block of heat-treated amorphous alloys," IEEE Transactions on Industry Applications, vol. 44, no. 3, pp. 699–706 (2008)

[16] Z. Wang, Y. Enomoto, M. Ito, R. Masaki, S. Morinaga, H. Itabashi, S. Tanigawa, "Development of a permanent magnet motor utilizing amorphous wound cores," IEEE Transactions on Magnetics, vol. 46, no. 2, pp. 570–573 (2010)

[17] Z. Wang, R. Masaki, S. Morinaga, Y. Enomoto, H. Itabashi, M. Ito, and S. Tanigawa, "Development of an axial gap motor with amorphous metal cores," IEEE Transactions on Industry Applications, vol. 47, no. 3, pp. 1293–1299 (2011)

[18] R. A. Caama˜no, "Electric motor or generator," U.S. Patent 5731649, Mar. 24 (1998)

[19] N. Ertugrul, R. Hasegawa, W. L. Soong, J. Gayler, S. Kloeden, and S. Kahourzade, "A novel tapered rotating electrical machine topology utilizing cut amorphous magnetic material," IEEE Transactions on Magnetics, vol. 51, no. 7, Art no. 8106006 (2015)

[20] T. Li, Y. Zhang, Y. Liang, Q. Ai, and H. Dou, "Multiphysics Analysis of an Axial-Flux In-Wheel Motor With an Amorphous Alloy Stator," IEEE Access, vol. 8, pp. 27414–27425 (2020)

[21] G. S. Liew, N. Ertugrul, W. L. Soong, J Gayler, "Investigation of axial field permanent magnet motor utilising amorphous magnetic material", Australian Journal of Electrical and Electronics Engineering, pp. 111-120 (2006)

[22] Hitachi News Release, "Highly Efficient Industrial 11kW Permanent Magnet Synchronous Motor without Rare-earth Metals —Realizing IE4 Class Efficiency Standard with a Smaller Motor—," http://www.hitachi.com/New/cnews /120411.html (2014)

[23] Y. Enomoto, H. Tokoi, T. Imagawa, T. Suzuki, T. Obata, and K. Souma, "Amorphous motor with IE5 efficiency class," Hitachi Review, vol. 64, no. 8, pp. 480–487, (2015)

[24] T. Sano, M. Takahashi, Y. Murakoshi, and K. Matsuno, "Punchless blanking of an amorphous alloy," Journal of Materials Processing Technology, 30, 341-350, (1992)

[25] F. Luo, F. Sun, K. Li, F. Gong, X. Liang, X. Wu, and Jiang Ma, "Ultrasonic assisted micro-shear punching of amorphous alloy," Materials Research Letters, 6:10, pp. 545-551 (2018)

[26] H. Li, Y. Yan, F. Sun, K. Li, F. Luo, and Jiang Ma, " Shear Punching of Amorphous Alloys under High-Frequency Vibrations," 9(11), 1158 (2019)

[27] J. Cui, H. Liu, Y. Ma, M. Li, J. Gong, Y. Zhang, X. Wang, "Flexible microblanking of amorphous alloys under laser dynamic loading," Journal of Manufacturing Processes, 56, pp.718-725 (2020)

[28] F. Takahashi, T. Nishimura, I. Suzuki, and H. Kudo, "A Method of Blanking from Amorphous Alloy Foils Using Rubber Tool," Annals of the CIRP, Vol.40, no.1, pp.315-318 (1991)

[29] Y. Murakoshi, M. Takahashi, M. Terasaki, T. Sano, and K. Matsuno, "High-speed blanking of an amorphous alloy," Journal of Materials Processing Technology, 30, 329-339 (1992)

[30] J. Ou, Y. Liu, P. Breining, M. Schiefer, M. Doppelbauer, "Experimental Study of the Amorphous Magnetic Material for High-Speed Sleeve-Free PM Rotor Application," IEEE Transactions on Industrial Electronics, Vol.67, no.6, pp.4422-4432 (2020)

[31] Miller T. J. E.: Switched reluctance motors and their control, pp.161-180, Magna Physics Publications and Oxford University Press (1993)